Asymptotic Global-Position Tracking Control of 3-D Fully Actuated Bipedal Robotic Walking ⋆

Yan Gu [a,*], Bin Yao [b], Yuan Gao [a], C. S. G. Lee [c]

[a] *Department of Mechanical Engineering, University of Masachusetts Lowell, Lowell, MA 01854, U.S.A.*

[b] *School of Mechanical Engineering, Purdue University, West Lafayette, IN 47907, U.S.A.*

[c] *School of Electrical and Computer Engineering, Purdue University, West Lafayette, IN 47907, U.S.A.*

Abstract

Bipedal robots are emerging as a critical technology for a wide range of applications such as disaster response and home assistance. This paper introduces a control approach that achieves asymptotic global-position tracking for three-dimensional (3-D) fully actuated bipedal robotic walking. Global-position tracking control is a challenging problem mainly due to the high complexity of the hybrid walking dynamics with state-triggered jumps and the time-varying nature of the desired global-position trajectory. Towards tackling this challenge, the first main contribution of this study is the construction of conditional impact invariance, which is used to design virtual constraints that satisfy a necessary condition required to realize asymptotic global-position tracking during 3-D walking. The second main contribution is the Lyapunov-based derivation of sufficient conditions under which the problem of global-position tracking control is provably solved for 3-D fully actuated bipedal robotic walking. Simulations and experiments on a fully actuated bipedal humanoid robot confirmed the validity of the proposed control approach in guaranteeing satisfactory global-position trajectory tracking.

Key words: nonlinear control, tracking, walking, robotics.

1 Introduction

Bipedal robots move through an environment by making and breaking contact with the ground. This unique form of locomotion is advantageous in traversing difficult surfaces (e.g., gaps, stairs, and ladders) that are common in applications such as disaster response and home assistance, and thus has motivated extensive research on bipedal walking control for achieving high-performance walking [14, 30, 31].

A safety-critical measure of walking performance is a bipedal robot's ability to track its desired time-varying position trajectory in an environment, which is herein terms as "global-position tracking". Poor global-position tracking can potentially put the safety of both humans and robots at risk, for example, by causing robots' failure to avoid pedestrians in human-populated environments.

Achieving reliable global-position tracking presents substantial controller design challenges mainly due to the high complexity of bipedal walking dynamics. A key challenge is the design of desired walking motions that a controller should reliably track. Bipedal walking dynamics are inherently hybrid involving state-triggered jumps, e.g., sudden jumps in joint velocities upon a foot-landing impact [10, 11, 20, 35]. Because these jumps cannot be directly controlled due to their infinitesimally short periods of duration, the robot's desired motions need to be designed to respect the impact dynamics (i.e., the jumps) for achieving asymptotic tracking. Yet, due to the high complexity of walking dynamics, the computational load of such design can be overly high for online implementation.

Another key challenge is the closed-loop stability analysis that provides conditions to guide controller design. Performing stability analysis is complicated because a controller capable of reliably tracking a time-varying global-position trajectory can result in a complex closed-loop system that is hybrid, nonlinear, and time-varying with uncontrolled, state-

⋆ Research by Y. Gu and Y. Gao was supported in part by NSF under Grant no. CMMI-1934280. The material in this paper was partially presented at the 2018 American Control Conference, June 27-29, Milwaukee, Wisconsin, U.S.A. and the 2019 American Control Conference, July 1-3, Philadelphia, Pennsylvania, U.S.A.

* Tel.: +1-978-934-5482.

Email addresses: yan_gu@uml.edu (Yan Gu), byao@purdue.edu (Bin Yao), yuan_gao@student.uml.edu (Yuan Gao), csglee@purdue.edu (C. S. G. Lee).

triggered jumps.

Previous work on tackling these two challenges is reviewed next.

1.1 Related Work

To achieve accurate global-position tracking, the Zero-Moment-Point (ZMP) control approach has been introduced based on the ZMP balance criterion [21, 23, 34]. Yet, the ZMP approach models a walking robot as a continuous dynamical system, and ignores the jumps in a robot's joint velocities caused by foot-landing impacts. This treatment can limit a controller's capabilities in realizing dynamic walking motions that typically involve significant impact behaviors.

In contrast to the ZMP approach, the Hybrid-Zero-Dynamics (HZD) approach [13, 27, 36] explicitly addresses the hybrid robot dynamics and stabilizes dynamic walking motions by provably stabilizing the hybrid closed-loop control system. This approach has realized remarkable locomotion performance on physical robots with various gait types such as periodic underactuated [19] and fully actuated walking [1] as well as aperiodic walking [6, 7, 29].

To tackle the challenge of designing desired walking motions that respect the impact dynamics for achieving asymptotic tracking, the HZD framework has introduced a constructive method that produces the needed desired motions. This method is derived through the design of virtual constraints that represent the relative evolution of a robot's posture (i.e., functions of joint positions) with respect to a phase variable that represents how far a step has progressed [36]. Recent studies have expanded this design from holonomic to non-holonomic constraints to produce desired motions for joint-velocity based control variables [12, 18]. However, these methods are not suitable for global-position tracking control because they only consider joint positions and motions but a robot's global position trajectory also depends on stance-foot position. Other recent virtual constraint designs are capable of guaranteeing stability of the constrained dynamics for general continuous systems [5, 26].

To solve the problem of analyzing the closed-loop stability for informing controller design, the HZD approach exploits the Poincaré section method to examine the asymptotic convergence of a robot's state to the periodic orbit corresponding to the desired motions. Yet, the resulting orbitally stabilizing controller cannot drive the state to converge to a prespecified time-varying trajectory that resides in the orbit [22]. Because a robot's desired global-position trajectory is often planned as an explicit time function in real-world applications, orbitally stabilizing control cannot directly guarantee asymptotic global-position tracking. Thus, it may not be valid to use the Poincaré section method to analyze the stability of a closed-loop system under global-position tracking control.

Towards enabling provable global-position tracking for 2-D fully actuated bipedal robotic walking, we have previously extended the virtual constraint design of the HZD framework to explicitly incorporate a 2-D robot's global position [15,16]. Based on the proposed virtual constraint design and Lyapunov-based stability analysis, we have derived sufficient conditions under which a continuous-phase control law provably achieves asymptotic global-position tracking.

Still, our previous control approach for 2-D walking, including the virtual constraint design and stability analysis, is not valid for 3-D walking. This is essentially because robot dynamics during 3-D walking are strongly nonlinearly coupled in the heading and lateral directions of the robot's global motion, whereas 2-D walking does not exhibit lateral motion and the coupling is accordingly trivial. This nonlinear coupling causes the substantially higher complexity of addressing 3-D walking as compared with 2-D walking.

Beyond the scope of global-position tracking control, trajectory tracking control of hybrid systems with state-triggered jumps has been actively studied [3,8,25,28,32,33]. Recently, Lyapunov-based controller design methodologies have been introduced to provably achieve asymptotic trajectory tracking [3, 8]. However, the evolution of the Lyapunov function across nonlinear state-triggered jumps, which are an inherent feature of robot walking dynamics, is not explicitly analyzed in these previous studies. Thus, it is not yet clear how to use these previous trajectory tracking control methods to directly inform the global-position tracking controller design for walking robots that possess highly nonlinear jumps.

1.2 Contributions

Towards tackling the challenges in achieving asymptotic global-position tracking for 3-D fully actuated bipedal walking, the key contributions of this study are summarized as follows:

i) Providing a constructive method of designing virtual constraints that can be used to greatly reduce the computational load in the generation of desired motions respecting impact dynamics.
ii) Establishing sufficient conditions based on Lyapunov stability analysis of the hybrid closed-loop system for guiding the design of continuous state-feedback control laws.
iii) Demonstrating the global-position tracking accuracy of the proposed control approach both through simulations and experimentally on a bipedal walking robot.
iv Validating the robustness of the proposed control design in addressing irregular walking surfaces such as moderately slippery floors.

Some of the results presented in this paper were initially reported in [17] and [9]. The present paper includes substantial, new contributions in the following aspects: a) the proof of the main theorem (i.e., Theorem 14) is updated with a new choice of Lyapunov function to properly analyze the convergence of the robot's lateral foot placement

during 3-D walking, and Proposition 12 is added along with its full proof, which supports the updated proof of the main theorem; b) fully developed proofs of all theorems, propositions, and corollaries are presented, which were missing in [17] and [9]; c) comparative experimental results are added to demonstrate the reliable global-position tracking performance of the proposed control approach; and d) robustness evaluation is newly included to illustrate the capability of the proposed control approach in handling relatively slippery walking surfaces.

This paper is structured as follows. Section 2 describes the problem formulation. The proposed continuous-phase tracking control law is explained in Section 3. Section 4 presents the proposed construction of conditional impact invariance for designing virtual constraints. The closed-loop stability analysis is introduced in Section 5. Proofs of all theorems, propositions, and corollaries are given in Section 6. Simulation and experimental results are reported in Section 7. Section 8 discusses potential directions of future work.

2 Problem Formulation

This section presents the problem formulation of the proposed controller design, including robot dynamics modeling, tracking error definition, and overall control objectives.

2.1 Full-Order Dynamic Modeling

This subsection presents a full-order model of bipedal walking dynamics that accurately describes the hybrid and nonlinear dynamic behaviors of all degrees of freedom (DOFs) involved in bipedal walking. The model serves as a basis for the proposed controller design.

The full-order model of bipedal walking dynamics is naturally hybrid because walking inherently involves both continuous behaviors (e.g., leg-swinging motions) and state-triggered discrete behaviors (e.g., the joint-velocity jumps upon swing-foot landings) [13].

The modeling assumptions include: a) the swing-foot landing impact is modeled as a contact between rigid bodies; b) upon a foot landing, the swing and the stance leg immediately switch roles, with the new swing leg beginning to move in the air and the new stance leg remaining in full, static contact with the ground until the next landing occurs; and c) all joints are independently actuated.

Under these assumptions, the robot is fully actuated; i.e., its full DOFs can be directly commanded to track any feasible trajectories within continuous walking phases. As illustrated in Fig. 1, a complete walking cycle can be decomposed into: a) a fully-actuated continuous phase during which one foot contacts the ground and the other moves in the air and b) a landing impact.

Note that this study focuses on the relatively simple gait, i.e., fully actuated gait, for two main reasons. First, asymptotic tracking of time-varying global-position trajectories is still an open control problem for this simple gait. Second, using a simple gait allows us to focus on solving the control challenges presented by the hybrid, nonlinear, time-varying closed-loop dynamics with state-triggered jumps.

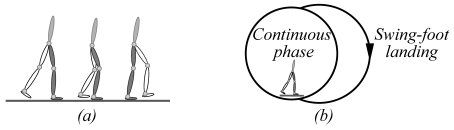

Fig. 1. An illustration of fully actuated bipedal robotic walking. (a) A gait cycle of fully actuated walking. (b) A fully actuated gait cycle is a hybrid process including a continuous phase and a discrete swing-foot landing.

Continuous-phase dynamics. Walking dynamics during continuous phases can be described by usual ordinary differential equations. Lagrange's method is used to obtain the following continuous-phase dynamic model [13]:

$$\mathbf{M}(\mathbf{q})\ddot{\mathbf{q}} + \mathbf{c}(\mathbf{q},\dot{\mathbf{q}}) = \mathbf{B}_u\mathbf{u}, \tag{1}$$

where $\mathbf{q} \in Q$ is the joint-position vector, $\mathbf{M} : Q \to \mathbb{R}^{n\times n}$ is the inertia matrix, $\mathbf{c} : TQ \to \mathbb{R}^n$ is the sum of Coriolis, centrifugal, and gravitational terms, $\mathbf{B}_u \in \mathbb{R}^{n\times m}$ is the joint-torque projection matrix, and $\mathbf{u} \in U$ is the joint-torque vector. Here, $Q \subset \mathbb{R}^n$ is the configuration space of the robot, TQ is the tangent space of Q, and $U \subset \mathbb{R}^m$ is the admissible joint-torque set. Note that $m = n$ when a robot is fully actuated.

Landing impact dynamics. When the swing foot lands on the ground, the swing leg and the stance leg switch roles, and an impulsive rigid-body impact occurs. Thus, both joint position and velocity vectors experience a sudden jump at a landing event. This state-triggered jump is described by the following reset map [13]:

$$\begin{bmatrix}\mathbf{q}^+\\ \dot{\mathbf{q}}^+\end{bmatrix} = \mathbf{\Delta}_{q,\dot{q}}(\mathbf{q}^-,\dot{\mathbf{q}}^-) := \begin{bmatrix}\mathbf{\Delta}_q(\mathbf{q}^-)\\ \mathbf{\Delta}_{\dot{q}}(\mathbf{q}^-)\dot{\mathbf{q}}^-\end{bmatrix}, \tag{2}$$

where $\star^-$ and $\star^+$ represent the values of $\star$ just before and just after the impact, respectively, and $\mathbf{\Delta}_{q,\dot{q}}$ represents the reset map.

Switching surface. A swing-foot landing event is triggered when the robot's state reaches the following switching surface $S_q(\mathbf{q},\dot{\mathbf{q}})$:

$$S_q(\mathbf{q},\dot{\mathbf{q}}) := \{(\mathbf{q},\dot{\mathbf{q}}) \in TQ : z_{sw}(\mathbf{q}) = 0,\ \dot{z}_{sw}(\mathbf{q},\dot{\mathbf{q}}) < 0\}, \tag{3}$$

where z_{sw} is the swing-foot height above the ground.

Combining the above equations yields the following full-order model of the hybrid, nonlinear walking dynamics with

state-triggered jumps:

$$\begin{cases} \mathbf{M}(\mathbf{q})\ddot{\mathbf{q}} + \mathbf{c}(\mathbf{q},\dot{\mathbf{q}}) = \mathbf{B}_u\mathbf{u}, & \text{if } (\mathbf{q}^-,\dot{\mathbf{q}}^-) \notin S_q(\mathbf{q},\dot{\mathbf{q}}); \\ \begin{bmatrix}\mathbf{q}^+ \\ \dot{\mathbf{q}}^+\end{bmatrix} = \boldsymbol{\Delta}_{q,\dot{q}}(\mathbf{q}^-,\dot{\mathbf{q}}^-), & \text{if } (\mathbf{q}^-,\dot{\mathbf{q}}^-) \in S_q(\mathbf{q},\dot{\mathbf{q}}). \end{cases} \quad (4)$$

A fully-actuated, n-DOF bipedal robot can track n independent desired position trajectories. The corresponding trajectory tracking errors are mathematically defined next.

2.2 Global-Position Tracking Error

Without loss of generality, a biped's base (e.g., chest) position (x_b, y_b, z_b) in the world reference frame $\Sigma_{X_wY_wZ_w}$ is chosen to represent its global position. For simplicity and without loss of generality, single-direction walking on horizontal flat surfaces is considered.

The horizontal components of the base position are:

$$x_b = x_{st} + \bar{x}_b(\mathbf{q}) \text{ and } y_b = y_{st} + \bar{y}_b(\mathbf{q}), \quad (5)$$

where $\bar{x}_b : Q \to Q_x \subset \mathbb{R}$ and $\bar{y}_b : Q \to Q_y \subset \mathbb{R}$ represent the x- and y-coordinates of the base position relative to the stance foot, respectively, and $(x_{st}, y_{st}, 0)$ denotes the stance-foot position in $\Sigma_{X_wY_wZ_w}$.

In real-world applications of robot locomotion, a path planner often provides the following desired motions:

a) The center line Γ_d of the desired global path.
b) The desired smooth position trajectory along Γ_d.

In this study, it is assumed that these desired motions have been specified by a higher-level planner.

For simplicity and without loss of generality, the center line Γ_d is specified as the X_w-axis of the world reference frame; i.e., $\Gamma_d = \{(x_b, y_b) \in \mathbb{R}^2 : y_b = 0\}$. Let $x_d(t)$ be the desired smooth position trajectory along Γ_d. Then, the global-position tracking error along Γ_d is defined as $\bar{x}_b(\mathbf{q}) - (x_d(t) - x_{st})$.

While $x_d(t)$ and Γ_d are often provided by a higher-level path planner in real-world robot applications, the desired base trajectory y_d in the lateral direction of Γ_d still needs to be defined, which is explained next.

2.3 Virtual-Constraint Tracking Error

In this study, we propose to use virtual constraints to define the desired trajectories for the lateral base position y_b and the remaining $n-2$ control variables $\boldsymbol{\phi}_c$.

Here, virtual constraints represent the relative evolution of a robot's posture and lateral global position with respect to a phase variable θ that represents how far a step has progressed. The phase variable is chosen as $\bar{x}_b(\mathbf{q})$; that is, $\theta = \bar{x}_b(\mathbf{q})$. The virtual constraints can be encoded by the phase variable θ as:

$$\begin{bmatrix}\bar{y}_b(\mathbf{q}) \\ \boldsymbol{\phi}_c(\mathbf{q})\end{bmatrix} - \begin{bmatrix}y_d(\theta(\mathbf{q})) - y_{st} \\ \boldsymbol{\phi}_d(\theta(\mathbf{q}))\end{bmatrix} = \mathbf{0}, \quad (6)$$

where $\boldsymbol{\phi}_c : Q \to Q_c \subset \mathbb{R}^{n-2}$ and $\theta : Q \to Q_f \subset \mathbb{R}$ are both continuously differentiable in $\mathbf{q}$. $y_d : Q_f \to \mathbb{R}$ and $\boldsymbol{\phi}_d : Q_f \to \mathbb{R}^{n-2}$ represent the desired trajectories of y_b and $\boldsymbol{\phi}_c$, respectively, and are both continuously differentiable in θ.

Then, the tracking error corresponding to the virtual constraints is defined as $\begin{bmatrix}\bar{y}_b(\mathbf{q}) \\ \boldsymbol{\phi}_c(\mathbf{q})\end{bmatrix} - \begin{bmatrix}y_d(\theta(\mathbf{q})) - y_{st} \\ \boldsymbol{\phi}_d(\theta(\mathbf{q}))\end{bmatrix}$.

2.4 Control Objective

The overall tracking error can be compactly expressed as:

$$\mathbf{h}(t,\mathbf{q}) = \mathbf{h}_c(\mathbf{q}) - \mathbf{h}_d(t,\mathbf{q}), \quad (7)$$

where $\mathbf{h}_c := \begin{bmatrix}\bar{x}_b & \bar{y}_b & \boldsymbol{\phi}_c^T\end{bmatrix}^T$ and $\mathbf{h}_d := \begin{bmatrix}x_d - x_{st} & y_d - y_{st} & \boldsymbol{\phi}_d^T\end{bmatrix}^T$.

Thus, the control objective is to drive $\mathbf{h}$ to zero for achieving asymptotic tracking of the desired trajectories, including the desired global-position trajectories, for 3-D bipedal robotic walking.

Our proposed control approach to achieve this objective is presented in the following sections.

3 Continuous-Phase Controller Design

This section presents a state-feedback control law that achieve asymptotic trajectory tracking during *continuous* phases. This control law is synthesized based on a full-order model of bipedal walking dynamics.

The proposed controller design begins with input-output linearization of the nonlinear continuous-phase dynamics, which then allows us to utilize the well-studied linear system theory to design the needed controller.

With the trajectory tracking error $\mathbf{h}$ chosen as the output function $\mathbf{y}$ (i.e., $\mathbf{y} = \mathbf{h}$), a continuous-phase control law is synthesized based on input-output linearization as [22]

$$\mathbf{u} = (\tfrac{\partial \mathbf{h}}{\partial \mathbf{q}}\mathbf{M}^{-1}\mathbf{B})^{-1}(\mathbf{v} + \tfrac{\partial \mathbf{h}}{\partial \mathbf{q}}\mathbf{M}^{-1}\mathbf{c} - \tfrac{\partial^2 \mathbf{h}}{\partial t^2} - \tfrac{\partial}{\partial \mathbf{q}}(\tfrac{\partial \mathbf{h}}{\partial \mathbf{q}}\dot{\mathbf{q}})\dot{\mathbf{q}}). \quad (8)$$

The continuous-phase dynamics then become $\ddot{\mathbf{y}} = \mathbf{v}$.

Choosing $\mathbf{v}$ as the following proportional-derivative (PD) control law [24]:

$$\mathbf{v} = -\mathbf{K}_P\mathbf{y} - \mathbf{K}_D\dot{\mathbf{y}}, \tag{9}$$

where the proportional gain matrix $\mathbf{K}_P \in \mathbb{R}^{n\times n}$ and the derivative gain matrix $\mathbf{K}_D \in \mathbb{R}^{n\times n}$ are both positive-definite diagonal matrices, one obtains the linear closed-loop dynamics of the output function during continuous phases as: $\ddot{\mathbf{y}} + \mathbf{K}_D\dot{\mathbf{y}} + \mathbf{K}_P\mathbf{y} = \mathbf{0}$.

Defining $\mathbf{x} := \begin{bmatrix}\mathbf{y}^T & \dot{\mathbf{y}}^T\end{bmatrix}^T \in \mathbb{R}^{2n}$, one obtains the closed-loop dynamics:

$$\begin{cases}\dot{\mathbf{x}} = \mathbf{A}\mathbf{x}, & \text{if } (t,\mathbf{x}^-) \notin S(t,\mathbf{x});\\ \mathbf{x}^+ = \boldsymbol{\Delta}(t,\mathbf{x}^-), & \text{if } (t,\mathbf{x}^-) \in S(t,\mathbf{x}),\end{cases} \tag{10}$$

where $\mathbf{A} := \begin{bmatrix}\mathbf{0}_{n\times n} & \mathbf{I}_{n\times n}\\ -\mathbf{K}_P & -\mathbf{K}_D\end{bmatrix}$. The expression of $S(t,\mathbf{x})$ can be obtained from Eqs. (3) and (7). The expression of $\boldsymbol{\Delta}$ can be obtained from Eq. (7) and that of $\boldsymbol{\Delta}_{q,\dot{q}}$. Note that $\boldsymbol{\Delta}$ is explicitly time-dependent because $\mathbf{h}$ is explicitly time-dependent.

The continuous-phase closed-loop dynamics (i.e., $\dot{\mathbf{x}} = \mathbf{A}\mathbf{x}$) will be asymptotically stable if the PD gains are chosen such that $\mathbf{A}$ is Hurwitz. Then, there exists a Lyapunov function candidate $V(\mathbf{x})$ for the continuous-phase dynamics and positive numbers c_1, c_2, and c_3 such that

$$c_1||\mathbf{x}||^2 \le V(\mathbf{x}) \le c_2||\mathbf{x}||^2 \text{ and } \dot{V}(\mathbf{x}) \le -c_3||\mathbf{x}||^2 \tag{11}$$

hold for all $\mathbf{x}$ during continuous phases [22].

Remark 1 *While the continuous-phase subsystem can be asymptotically stabilized by properly choosing the PD gains, the impact (i.e., $\mathbf{x}^+ = \boldsymbol{\Delta}(t,\mathbf{x}^-)$) cannot be directly controlled due to its infinitesimal period of duration. Thus, the desired trajectories need to be designed to respect the impact dynamics, which is a necessary condition for achieving asymptotic trajectory tracking. Also, the stability of the hybrid closed-loop system in Eq.* (10) *needs to be analyzed in order to guide the tuning of the control gains. Both tasks are complicated due to the high complexity of the uncontrolled, nonlinear, time-varying closed-loop impact dynamics. Our proposed methods to solve these tasks are explained next.*

4 Conditional Impact Invariance Construction for Synthesizing Virtual Constraints

This section presents the proposed construction of conditional impact invariance for designing the virtual constraints in Eq. (6).

The goal of the design is to ensure that the robot's full desired motions respect the impact dynamics, which is a necessary condition required to achieve asymptotic trajectory tracking for the hybrid closed-loop system in Eq. (10). The full desired motions comprise: a) the desired global-position trajectory $x_d(t)$, which has been provided by a higher-level planner, and b) the desired functions y_d and $\boldsymbol{\phi}_d$, which are associated with the virtual constraints to be designed.

Definition 2 *The output function $\mathbf{y}$ and its derivative $\dot{\mathbf{y}}$ are impact invariant if the following condition is met: $\mathbf{y}^+ = \mathbf{0}$ and $\dot{\mathbf{y}}^+ = \mathbf{0}$ hold when $\mathbf{y}^- = \mathbf{0}$ and $\dot{\mathbf{y}}^- = \mathbf{0}$ hold just before an impact event [27, 36].*

Satisfying the impact invariance condition at the steady state is a necessary condition for achieving asymptotic trajectory (and orbit) tracking for hybrid systems with state-triggered jumps. Suppose that the impact invariance condition is not satisfied at the steady state. Then, because the robot's impact dynamics cannot be directly regulated, the output function $\mathbf{y}$ (i.e., the tracking error $\mathbf{h}$) and its derivative may become nonzero just after an impact even if they are both zero just before the impact, which means the asymptotic tracking cannot be achieved.

Definition 3 *Let T_k be the timing of the k^{th} ($k \in \{1,2,...\}$) actual landing impact, which is defined as the timing of the first intersection between $\mathbf{x}$ and $S(t,\mathbf{x})$ on $t > T_{k-1}^+$. Without loss of generality, define $T_0 = 0$. Let τ_k denote the k^{th} ($k \in \{1,2,...\}$ desired impact timing, which is defined as the timing of the first intersection between $\mathbf{x}$ and the switching surface $S(t,\mathbf{x})$ on $t > T_{k-1}^+$ assuming $\mathbf{x} = \mathbf{0}$ $\forall t > T_{k-1}^+$.*

For the rest of the paper, $\star(T_{k-1}^-)$ and $\star(T_{k-1}^+)$ will be denoted as $\star|_{k-1}^-$ and $\star|_{k-1}^+$, respectively, when notational simplicity is preferred.

Assumption 4 *Let (x_{sw}, y_{sw}, z_{sw}) be the swing-foot position in the world reference frame. Let $\phi_{sw,z}(\theta)$ be an component of $\boldsymbol{\phi}_d(\theta)$ that represents the desired trajectory of z_{sw}. The desired function $\phi_{sw,z}(\theta)$ has at least one intersection with zero for $\theta < 0$ and $\theta > 0$, respectively.*

Assumption 5 *There exists a diffeomorphism $D : Q_c \times Q_f \times Q_y \to Q$.*

Assumption 6 *Define $\mathbf{H}_v(\mathbf{q}) := \left[\frac{d\bar{x}_b}{d\mathbf{q}}^T(\mathbf{q}) \ \frac{d\bar{y}_b}{d\mathbf{q}}^T(\mathbf{q}) \ \frac{d\boldsymbol{\phi}_c}{d\mathbf{q}}^T(\mathbf{q})\right]^T$. Define $\mathbf{q}_0 := \boldsymbol{\Delta}_q(\mathbf{q}^*)$ and $\theta_0 := \bar{x}_b(\mathbf{q}_0)$. $\mathbf{H}_v(\mathbf{q})$ is locally invertible within a small neighborhood about $\mathbf{q}^*$.*

Remark 7 *Assumptions 4 and 5 can be satisfied through the trajectory generation of y_d and $\boldsymbol{\phi}_d$, which are both used to define the virtual constraints in Eq.* (6)*. Assumption 6 can be met by choosing $\boldsymbol{\phi}_c$ to be independent from $\bar{x}_b$ and $\bar{y}_b$.*

Proposition 8 *Let Assumptions 4 and 5 hold. Let $\phi_{sw,y}(\theta)$ be an component of $\boldsymbol{\phi}_d(\theta)$ that represents the desired trajectory of the lateral swing-foot position y_{sw}. When the lateral stance-foot position satisfies the condition $y_{st} = y_{std} :=$*

$\phi_{sw,y}(\theta^*)$, *there exists a constant* θ^* *such that* $\theta(\tau_k^-) = \theta^*$, $\bar{y}_b(\tau_k^-) = y_d(\theta^*) - y_{std}$, *and* $\boldsymbol{\phi}_c(\tau_k^-) = \boldsymbol{\phi}_d(\theta^*)$ *always hold when* $\mathbf{x} = \mathbf{0}\ \forall t > T_{k-1}^+$ ($k \in \{1,2,...\}$). *Furthermore,* $\mathbf{q}(\tau_k^-) \in Q$ *has a fixed value, denoted as* $\mathbf{q}^*$.

Theorem 9 (Conditional Impact Invariance Construction) *Let Assumption 6 hold. Suppose that the desired functions* y_d *and* $\boldsymbol{\phi}_d$ *are planned with Assumptions 4 and 5 satisfied along with the following conditions:*

(B1) $\bar{y}_b(\mathbf{q}_0) = y_d(\theta_0) - y_{std}$ *and* $\boldsymbol{\phi}_c(\mathbf{q}_0) = \boldsymbol{\phi}_d(\theta_0)$.

(B2) $$\frac{d\bar{x}_b}{d\mathbf{q}}(\mathbf{q}_0)\boldsymbol{\Delta}_{\dot{q}}(\mathbf{q}^*)\mathbf{H}_v^{-1}(\mathbf{q}^*)\begin{bmatrix} 1 \\ \frac{dy_d}{d\theta}(\theta^*) \\ \frac{d\boldsymbol{\phi}_d}{d\theta}(\theta^*) \end{bmatrix} = 1.$$

(B3) $$\mathbf{H}_v(\mathbf{q}_0)\boldsymbol{\Delta}_{\dot{q}}(\mathbf{q}^*)\mathbf{H}_v^{-1}(\mathbf{q}^*)\begin{bmatrix} 1 \\ \frac{dy_d}{d\theta}(\theta^*) \\ \frac{d\boldsymbol{\phi}_d}{d\theta}(\theta^*) \end{bmatrix} = \begin{bmatrix} 1 \\ \frac{dy_d}{d\theta}(\theta_0) \\ \frac{d\boldsymbol{\phi}_d}{d\theta}(\theta_0) \end{bmatrix}.$$

Then, under the lateral foot-placement condition $y_{st} = y_{std}$, *impact invariance holds; that is, if* $\mathbf{x}(\tau_k^-) = \mathbf{0}$ *then* $\mathbf{x}(\tau_k^+) = \boldsymbol{\Delta}(\tau_k, \mathbf{0}) = \mathbf{0}$.

Remark 10 *If the virtual constraints in Eq.* (6) *are designed with the desired functions* y_d *and* $\boldsymbol{\phi}_d$ *satisfying the conditions in Theorem 9, then the robot's desired motions will respect the impact dynamics under the lateral foot-placement condition* $y_{st} = y_{std}$ *during 3-D walking. Section 5 will provide sufficient conditions under which the proposed continuous control law ensures that this foot-placement condition indeed holds at the steady state during actual walking.*

Remark 11 *Theorem 9 indicates that the satisfaction of the impact invariance condition only relies on the design of the virtual constraints in Eq.* (6) *but does not depend on the arbitrary global-position trajectory* x_d *provided by a higher-level planner. For this reason, the design of virtual constraints can be performed offline, thus greatly reducing the computational load for online implementation.*

5 Closed-loop Stability Analysis

This section introduces the Lyapunov-based stability analysis of the hybrid, nonlinear, time-varying closed-loop tracking error dynamics in Eq. (10) under the proposed continuous-phase control law in Eqs. (8) and (9) as well as the proposed synthesis of virtual constraints summarized in Theorem 9. The outcome of this stability analysis will be a set of sufficient conditions under which the proposed control law provably guarantees asymptotic closed-loop trajectory tracking.

Before presenting the main theorem on closed-loop stability, we first derive the boundedness of the lateral stance-foot position y_{st}.

Proposition 12 (Boundedness of Lateral Foot Placement) *Let* $\tilde{\mathbf{x}}(t;t_0,\lambda_0)$ *be a solution of a fictitious system* $\dot{\tilde{\mathbf{x}}} = \mathbf{A}\tilde{\mathbf{x}}$ *with the initial condition* $\tilde{\mathbf{x}}(t_0) = \lambda_0,\ \forall t > t_0$. *There exist positive numbers* β_{st} *and* d_1 *such that for any* $\mathbf{x}|_0^+ \in B_{d_1}(\mathbf{0}) := \{\mathbf{x} \in \mathbb{R}^{2n} : \|\mathbf{x}\| \le d_1\}$

$$|y_{st}|_k^+ - y_{std}| \le \|\mathbf{x}|_k^-\| + \beta_{st}\|\tilde{\mathbf{x}}(\tau_k; T_{k-1}^+, \mathbf{x}|_{k-1}^+)\| \qquad (12)$$

holds ($k \in \{1,2,...\}$).

Remark 13 *Proposition 12 shows that the deviation of the lateral foot placement during an actual 3-D walking process is bounded above by the norms of the actual state* $\mathbf{x}$ *and the fictitious state* $\tilde{\mathbf{x}}$. *This indicates that driving* $\mathbf{x}$ *and* $\tilde{\mathbf{x}}$ *to zero will indirectly eliminate this deviation and thus meet the lateral foot-placement condition underlying the proposed virtual constraint design in Theorem 9.*

Theorem 14 (Closed-Loop Stability Conditions) *Let Assumptions 4-6 and the conditions (B1)-(B3) hold. The closed-loop control system in Eq.* (10) *is locally asymptotically stable if the PD gains in Eq.* (9) *are chosen such that* $\mathbf{A}$ *is Hurwitz and that the continuous-phase convergence rate is sufficiently fast.*

Theorem 14 confirms the validity of using the proposed continuous-phase control law to explicitly address the hybrid walking dynamics for achieving asymptotic global-position tracking during fully actuated 3-D bipedal robotic walking. It also provides sufficient conditions that can be used to guide the controller design in terms of choosing the PD gains, as summarized in the following remark.

Remark 15 *The proof of Theorem 14 (Section 6.4) provides a lower bound of the continuous-phase convergence rate for guaranteeing asymptotic trajectory tracking of the hybrid closed-loop system. This lower bound is given in Eq.* (35). *While it is straightforward to choose the PD gains such that* $\mathbf{A}$ *is Hurwitz, to meet the conditions in Eq.* (35) *requires the construction of* $V(\mathbf{x})$. *For example,* $V(\mathbf{x})$ *can be constructed as* $V(\mathbf{x}) = \mathbf{x}^T\mathbf{P}\mathbf{x}$, *where* $\mathbf{P}$ *is the solution to the Lyapunov equation* $\mathbf{P}\mathbf{A} + \mathbf{A}^T\mathbf{P} = -\mathbf{Q}$ *[22]. Here,* $\mathbf{Q}$ *is any positive definite symmetric matrix satisfying* $\mathbf{0} < \lambda_Q\mathbf{I} \le \mathbf{Q}$ *with a positive number* λ_Q. *For simplicity,* $\mathbf{Q}$ *can be chosen as an identity matrix, and then* λ_Q *can be any number satisfying* $0 < \lambda_Q \le 1$. *Then, the bounds in Eq.* (11) *can be assigned as* $c_1 = \lambda_{min}(\mathbf{P})$, $c_2 = \lambda_{max}(\mathbf{P})$, *and* $c_3 = \lambda_Q$, *where* $\lambda_{min}(\mathbf{P})$ *and* $\lambda_{max}(\mathbf{P})$ *are the smallest and the largest eigenvalues of* $\mathbf{P}$, *respectively. With* V *constructed, the PD gains can be specified to meet the two inequality conditions in Eq.* (35). *From the second inequality in Eq.* (35), σ *can be specified as any number satisfying* $\sigma > 2\lambda_{max}(\mathbf{P})\alpha_{st}$, *where* α_{st} *can be estimated from system dynamics. Then, the PD gains can be specified to satisfy the first inequality in Eq.* (35). *Specifically, the PD gains should produce a sufficiently high continuous-phase convergence rate* $\frac{c_3}{2c_2}$, *i.e.,* $\frac{\lambda_Q}{2\lambda_{max}(\mathbf{P})}$, *such that* α_x *and* γ_x *are sufficiently small to make the first inequality in Eq.* (35) *hold.*

Corollary 16 (Convergence of Lateral Foot Placement) *When the closed-loop system in Eq.* (10) *is asymptotically stable under the control approach summarized in Theorem 14, the lateral foot-placement condition $y_{st} = y_{std}$ will hold at the steady state.*

Remark 17 *Corollary 16 indicates that the lateral foot-placement condition underlying the proposed conditional impact invariance construction in Theorem 9 is indeed met at the steady state. Then, by Corollary 16 and Theorem 9, if $\mathbf{x}(\tau_k^-) \to \mathbf{0}$ then $\mathbf{x}(\tau_k^+) = \mathbf{\Delta}(\tau_k, \mathbf{0}) \to \mathbf{0}$ as $k \to \infty$.*

Corollary 18 (Convergence of Impact Timing) *When the closed-loop system in Eq.* (10) *is asymptotically stable under the control approach summarized in Theorem 14, the actual impact timing T_k will asymptotically converge to the desired timing τ_k.*

Remark 19 *In contrast to the proposed global-position tracking control, an orbitally stabilizing controller cannot achieve asymptotic tracking of the desired global position trajectories, as explained in Section 1.1. Accordingly, it cannot realize asymptotic convergence to the desired timing τ_k but can realize a finite final error for $T_k - \tau_k$.*

6 Proofs of Propositions, Theorems, and Corollaries

6.1 Proof of Proposition 8

PROOF. By the definitions of τ_k and the switching surface, one has $z_{sw}(\tau_k^-) = 0$. By the definition of $\mathbf{x}$, one has $z_{sw}(\tau_k^-) = \phi_{sw,z}(\theta(\tau_k^-))$ when $\mathbf{x} = 0 \ \forall t > T_{k-1}^+$. Thus,

$$\phi_{sw,z}(\theta(\tau_k^-)) = 0. \tag{13}$$

Because θ monotonically evolves and crosses zero during a single-direction walking step and because $\phi_{sw,z}(\theta)$ has at least one intersection with zero for $\theta < 0$ and $\theta > 0$ (i.e., Assumption 4), Eq. (13) indicates that $\theta(\tau_k^-)$ has a fixed value; i.e., there exists a constant θ^* such that $\theta(\tau_k^-) = \theta^*$ always holds. Accordingly, $\bar{y}_b(\tau_k^-) = y_d(\theta^*) - y_{std}$ and $\boldsymbol{\phi}_c(\tau_k^-) = \boldsymbol{\phi}_d(\theta^*)$ always hold. Thus, under Assumption 5,

$$\left[\boldsymbol{\phi}_c^T(\mathbf{q}) \ \bar{x}_b(\mathbf{q}) \ \bar{y}_b(\mathbf{q})\right]^T = \left[\boldsymbol{\phi}_d^T(\theta^*) \ \theta^* \ -y_{std}\right]^T$$

has a unique solution on $\mathbf{q} \in Q$, denoted as $\mathbf{q}^*$, when $y_{st} = y_{std}$.

6.2 Proof of Theorem 9

PROOF. From Proposition 8 and $\mathbf{x}(\tau_k^-) = \mathbf{0}$, one has $\mathbf{q}(\tau_k^+) = \mathbf{q}_0$ and $\theta(\tau_k^+) = \theta_0$. Then, from (B1), one has

$$\bar{y}_b(\mathbf{q}_0) - y_d(\theta_0) + y_{st} = 0 \text{ and } \boldsymbol{\phi}_c(\mathbf{q}_0) - \boldsymbol{\phi}_d(\theta_0) = \mathbf{0}. \tag{14}$$

Because $\mathbf{x}(\tau_k^-) = \mathbf{0}$ and because x_b and $x_d(t)$ are continuous in t, one has

$$\bar{x}_b(\mathbf{q}_0) - x_d(\tau_k^+) + x_{st} = 0 \tag{15}$$

From Eqs. (14) and (15), $\mathbf{y}(\tau_k^+) = \mathbf{h}(\tau_k^+) = \mathbf{0}$ holds.

Because $\dot{\mathbf{y}}(\tau_k^-) = \mathbf{0}$, one has

$$\mathbf{H}_v(\mathbf{q}^*)\dot{\mathbf{q}}(\tau_k^-) = \begin{bmatrix} 1 \\ \frac{dy_d}{d\theta}(\theta^*) \\ \frac{d\boldsymbol{\phi}_d}{d\theta}(\theta^*) \end{bmatrix} \dot{\theta}(\tau_k^-). \tag{16}$$

From Eq. (2), one has

$$\dot{\mathbf{q}}(\tau_k^+) = \mathbf{\Delta}_{\dot{q}}(\mathbf{q}^*)\dot{\mathbf{q}}(\tau_k^-).$$

Because the stance foot remains static within a step, one has $\dot{x}_d^+ = \dot{x}_d^- = \dot{\theta}(\tau_k^-)$. Then, by the definition of $\mathbf{y}$, one has

$$\dot{\mathbf{y}}(\tau_k^+) = \mathbf{H}_v(\mathbf{q}_0)\dot{\mathbf{q}}(\tau_k^+) - \begin{bmatrix} \dot{\theta}(\tau_k^-) \\ \frac{dy_d}{d\theta}^T(\theta_0)\dot{\theta}(\tau_k^+) \\ \frac{d\boldsymbol{\phi}_d}{d\theta}^T(\theta_0)\dot{\theta}(\tau_k^+) \end{bmatrix}.$$

From (B2), one has

$$\dot{\theta}(\tau_k^+) = \frac{d\bar{x}_b}{d\mathbf{q}}(\mathbf{q}_0)\dot{\mathbf{q}}(\tau_k^+) = \dot{\theta}(\tau_k^-). \tag{17}$$

From (B3) and Eqs. (16)-(17), $\dot{\mathbf{y}}(\tau_k^+) = \mathbf{0}$ holds.

6.3 Proof of Proposition 12

PROOF. Because the stance-foot position during the $k+1^{th}$ step is the swing-foot position at the end of the k^{th} step, one has

$$y_{st}|_k^+ = y_{sw}|_k^-.$$

Recall $y_{std} := \phi_{sw,y}(\theta^*)$. Then,

$$\begin{aligned} &|y_{st}|_k^+ - y_{std}| = |y_{sw}|_k^- - \phi_{sw,y}(\theta^*)| \\ &\leq |y_{sw}|_k^- - \phi_{sw,y}(\theta(T_k^-))| \\ &\quad + |\phi_{sw,y}(\theta(T_k^-)) - \phi_{sw,y}(\tilde{\theta}(\tau_k; T_{k-1}^+, \mathbf{x}|_{k-1}^+))| \\ &\quad + |\phi_{sw,y}(\tilde{\theta}(\tau_k; T_{k-1}^+, \mathbf{x}|_{k-1}^+)) - \phi_{sw,y}(\theta^*)|. \end{aligned} \tag{18}$$

By the definition of $\mathbf{y}$, one has

$$|y_{sw}|_k^- - \phi_{sw,y}(\theta(T_k^-))| \leq \|\mathbf{x}|_k^-\|. \tag{19}$$

Recall $\theta(T_k^-) = \tilde{\theta}(T_k; T_{k-1}^+, \mathbf{x}|_{k-1}^+)$. Because $\phi_{sw,y}(\theta)$ and $\tilde{\theta}(t; T_{k-1}^+, \mathbf{x}|_{k-1}^+)$ are continuously differentiable in θ and t, respectively, there exists a positive number r_1 and Lipschitz constants $L_{\phi_{sw,y}}$ and L_{θ_t} such that

$$\begin{aligned} &\|\phi_{sw,y}(\theta(T_k^-)) - \phi_{sw,y}(\tilde{\theta}(\tau_k; T_{k-1}^+, \mathbf{x}|_{k-1}^+))\| \\ &\leq L_{\phi_{sw,y}} \|\theta(T_k^-) - \tilde{\theta}(\tau_k; T_{k-1}^+, \mathbf{x}|_{k-1}^+)\| \\ &\leq L_{\phi_{sw,y}} L_{\theta_t} |T_k - \tau_k| \end{aligned} \tag{20}$$

By [Theorem 1, [16]], there exists a positive number r_2 and a Lipschitz constant L_{T_x} such that

$$|T_k - \tau_k| \leq L_{T_x} \|\tilde{\mathbf{x}}(\tau_k; T_{k-1}^+, \mathbf{x}|_{k-1}^+)\| \tag{21}$$

for any $\mathbf{x}|_0^+ \in B_{r_2}(\mathbf{0})$.

Because

$$\theta^* = \tilde{\theta}(\tau_k^-; T_{k-1}^+, \mathbf{0}) = x_d(\tau_k) - x_{st}|_k^-,$$

one has

$$\begin{aligned} &|\tilde{\theta}(\tau_k; T_{k-1}^+, \mathbf{x}|_{k-1}^+) - \theta^*| \\ &= \|\tilde{\mathbf{x}}_b(\tau_k; T_{k-1}^+, \mathbf{x}|_{k-1}^+) - (x_d(\tau_k) - x_{st}|_k^-)\| \\ &\leq \|\tilde{\mathbf{x}}(\tau_k; T_{k-1}^+, \mathbf{x}|_{k-1}^+)\|. \end{aligned} \tag{22}$$

Let $\beta = L_{\phi_{sw,y}}(L_{\theta_t} L_{T_x} + 1)$ and $d_1 = \min(r_1, r_2)$. Then, from Eqs. (18)-(22), one obtains

$$|y_{st}|_k^+ - y_{std}| \leq \|\mathbf{x}|_k^-\| + \beta_{st} \|\tilde{\mathbf{x}}(\tau_k; T_{k-1}^+, \mathbf{x}|_{k-1}^+)\| \tag{23}$$

for any $\mathbf{x}|_0^+ \in B_{d_1}(\mathbf{0})$.

6.4 Proof of Theorem 14

PROOF. To simplify the stability analysis using the proposed conditional impact invariance, which holds when $y_{st} = y_{std}$, we will explicitly analyze the convergence of y_{st} to y_{std}. Thus, an augmented Lyapunov function candidate is constructed as

$$V_a(\mathbf{x}, y_{st} - y_{std}) := V(\mathbf{x}) + \sigma(y_{st} - y_{std})^2, \tag{24}$$

where σ is a positive number to be specified later.

By the stability theory based on the construction of multiple Lyapunov functions [4], the hybrid time-varying system in Eq. (10) is locally asymptotically stable if there exists a positive number d_2 such that, for any $\mathbf{x}|_0^+ \in B_{d_2}(\mathbf{0})$, V_a is monotonically decreasing during each continuous phase and $\{V_a|_1^+, V_a|_2^+, V_a|_3^+ ...\}$ is a strictly decreasing sequence with $V_a|_k^+ \to 0$ as $k \to \infty$.

Evolution of V_a during continuous phases. Choose the PD gains such that $\mathbf{A}$ is Hurwitz. Then, Eq. (11) yields

$$V|_k^- \leq e^{-\frac{c_3}{c_2}(T_{k+1} - T_k)} V|_{k-1}^+$$

for the k^{th} ($k \in \{1, 2, ...\}$) walking step. Also, $y_{st} - y_{std}$ remains constant within the step because the stance foot is static. Thus, V_a is monotonically decreasing during the k^{th} step.

Evolution of V_a across nonlinear jumps. Consider the foot-landing event at the end of the k^{th} walking step (i.e., $t = T_k^-$). The tracking error convergence across the landing event is analyzed as follows, with the effect of y_{st} on the convergence explicitly discussed.

Because the desired function $\boldsymbol{\phi}_d(\theta)$ satisfies the conditions (B1)-(B3), the proposed conditional impact invariance (i.e., Theorem 2) holds. Thus, $\boldsymbol{\Delta}(\tau_k^-, \mathbf{0}, y_{std}) = \mathbf{0}$.

Thus, the value of $\mathbf{x}$ just after the landing can be approximated as:

$$\begin{aligned} \|\mathbf{x}|_k^+\| &= \|\boldsymbol{\Delta}(T_k^-, \mathbf{x}|_k^-, y_{st}|_k^-)\| \\ &= \|\boldsymbol{\Delta}(T_k^-, \mathbf{x}|_k^-, y_{st}|_k^-) - \boldsymbol{\Delta}(\tau_k^-, \mathbf{0}, y_{std})\| \\ &\leq \|\boldsymbol{\Delta}(T_k^-, \mathbf{x}|_k^-, y_{st}|_k^-) - \boldsymbol{\Delta}(\tau_k^-, \mathbf{x}|_k^-, y_{st}|_k^-)\| \\ &\quad + \|\boldsymbol{\Delta}(\tau_k^-, \mathbf{x}|_k^-, y_{st}|_k^-) - \boldsymbol{\Delta}(\tau_k^-, \mathbf{0}, y_{st}|_k^-)\| \\ &\quad + \|\boldsymbol{\Delta}(\tau_k^-, \mathbf{0}, y_{st}|_k^-) - \boldsymbol{\Delta}(\tau_k^-, \mathbf{0}, y_{std})\| \\ &\quad + \|\boldsymbol{\Delta}(\tau_k^-, \mathbf{0}, y_{std})\|. \end{aligned} \tag{25}$$

Because the reset map $\boldsymbol{\Delta}(t, \mathbf{x}, y_{st})$ is continuously differentiable in t, $\mathbf{x}$, and y_{st}, there exists a positive number r_3 and Lipschitz constants L_{Δ_t}, L_{Δ_x}, and $L_{\Delta_{st}}$ such that the following inequalities hold for any $\mathbf{x}|_0^+ \in B_{r_3}(\mathbf{0})$:

$$\begin{aligned} &\|\boldsymbol{\Delta}(T_k^-, \mathbf{x}|_k^-, y_{st}|_k^-) - \boldsymbol{\Delta}(\tau_k^-, \mathbf{x}|_k^-, y_{st}|_k^-)\| \leq L_{\Delta_t} |T_k - \tau_k|. \\ &\|\boldsymbol{\Delta}(\tau_k^-, \mathbf{x}|_k^-, y_{st}|_k^-) - \boldsymbol{\Delta}(\tau_k^-, \mathbf{0}, y_{st}|_k^-)\| \leq L_{\Delta_x} \|\mathbf{x}|_k^-\|. \\ &\|\boldsymbol{\Delta}(\tau_k^-, \mathbf{0}, y_{st}|_k^-) - \boldsymbol{\Delta}(\tau_k^-, \mathbf{0}, y_{std})\| \leq L_{\Delta_{st}} |y_{st}|_k^- - y_{std}|. \end{aligned} \tag{26}$$

From Eqs. (21) and (26), one has

$$\begin{aligned} &\|\boldsymbol{\Delta}(T_k^-, \mathbf{x}|_k^-, y_{st}|_k^-) - \boldsymbol{\Delta}(\tau_k^-, \mathbf{x}|_k^-, y_{st}|_k^-)\| \\ &\leq L_{\Delta_t} L_{T_x} \|\tilde{\mathbf{x}}(\tau_k; T_{k-1}^+, \mathbf{x}|_{k-1}^+)\| \end{aligned} \tag{27}$$

for any $\mathbf{x}|_0^+ \in B_{d_2}(\mathbf{0})$, where $d_2 = \min\{d_1, r_3\}$.

From Eqs. (25) - (27), one has, for any $\mathbf{x}|_0^+ \in B_{d_2}(\mathbf{0})$,

$$\begin{aligned} &\|\mathbf{x}|_k^+\| = \|\boldsymbol{\Delta}(T_k^-, \mathbf{x}|_k^-, y_{st}|_k^-)\| \\ \leq\ & L_{\Delta_t} L_{T_x} \|\tilde{\mathbf{x}}(\tau_k; T_{k-1}^+, \mathbf{x}|_{k-1}^+)\| + L_{\Delta_x} \|\mathbf{x}|_k^-\| + L_{\Delta_{st}} |y_{st}|_k^- - y_{std}|. \end{aligned} \tag{28}$$

From Eq. (11), one has:

$$\begin{aligned} &\|\mathbf{x}|_k^-\| \leq \sqrt{\tfrac{c_2}{c_1}} e^{-\frac{c_3}{2c_2}(T_k - T_{k-1})} \|\mathbf{x}|_{k-1}^+\|. \\ &\|\tilde{\mathbf{x}}(\tau_k; T_{k-1}^+, \mathbf{x}|_{k-1}^+)\| \leq \sqrt{\tfrac{c_2}{c_1}} e^{-\frac{c_3}{2c_2}(\tau_k - T_{k-1})} \|\mathbf{x}|_{k-1}^+\|. \end{aligned} \tag{29}$$

Then, from Eqs. (28) and (29), one has

$$\begin{aligned} \|\mathbf{x}|_k^+\| \leq & \sqrt{\tfrac{c_2}{c_1}} (L_{\Delta_t} L_{T_x} + L_{\Delta_x} e^{-\frac{c_3}{2c_2}(T_k - \tau_k)}) e^{-\frac{c_3}{2c_2}(\tau_k - T_{k-1})} \|\mathbf{x}|_{k-1}^+\| \\ & + L_{\Delta_{st}} |y_{st}|_k^- - y_{std}|. \end{aligned} \tag{30}$$

For any $\varepsilon > 0$ there exist PD gains corresponding to a sufficiently high convergence rate $\frac{c_3}{2c_2}$ such that

$$e^{-\frac{c_3}{2c_2}(T_k - \tau_k)} \leq 1 + \varepsilon. \tag{31}$$

From Eqs. (30) and (31), for any $\mathbf{x}|_0^+ \in B_{d_2}(\mathbf{0})$ one has

$$\|\mathbf{x}|_k^+\| \leq \alpha_x \|\mathbf{x}|_{k-1}^+\| + \alpha_{st} |y_{st}|_k^- - y_{std}|. \tag{32}$$

where $\alpha_x := \sqrt{\frac{c_2}{c_1}} (L_{\Delta_t} L_{T_x} + L_{\Delta_x}(1+\varepsilon)) e^{-\frac{c_3}{2c_2}\Delta\tau_k}$, $\Delta\tau_k := \tau_k - T_{k-1}$, and $\alpha_{st} := L_{\Delta_{st}}$. Because the stance foot remains static within a step, one has $y_{st}|_k^- = y_{st}|_{k-1}^+$.

From Eq. (12), one has

$$|y_{st}|_k^+ - y_{std}| \leq \|\mathbf{x}|_k^-\| + \beta_{st} \|\tilde{\mathbf{x}}(\tau_k; T_{k-1}^+, \mathbf{x}|_{k-1}^+)\| \leq \gamma_x \|\mathbf{x}|_{k-1}^+\| \tag{33}$$

where $\gamma_x := \sqrt{\frac{c_2}{c_1}} (\beta_{st} + (1+\varepsilon)) e^{-\frac{c_3}{2c_2}\Delta\tau_k}$.

From Eqs. (11), (24), (32), and (33), one has

$$\begin{aligned} V_a|_k^+ &= V|_k^+ + \sigma(y_{st}|_k^+ - y_{std})^2 \\ &\leq c_2 \|\mathbf{x}|_k^+\|^2 + \sigma(y_{st}|_k^+ - y_{std})^2 \\ &\leq B(c_1 \|\mathbf{x}|_{k-1}^+\|^2 + \sigma(y_{st}|_{k-1}^+ - y_{std})^2) \\ &\leq B(V|_{k-1}^+ + \sigma(y_{st}|_{k-1}^+ - y_{std})^2) \leq B V_a|_{k-1}^+, \end{aligned} \tag{34}$$

where $B := \max(\frac{2c_2\alpha_x^2 + \sigma\gamma_x^2}{c_1}, \frac{2c_2\alpha_{st}}{\sigma})$.

If the PD gains and σ are chosen such that

$$\tfrac{2c_2\alpha_x^2 + \sigma\gamma_x^2}{c_1} < 1 \text{ and } \tfrac{2c_2\alpha_{st}}{\sigma} < 1 \tag{35}$$

hold (i.e., $B < 1$), then for any $\mathbf{x}|_0^+ \in B_{d_2}(\mathbf{0})$ the sequence $\{V_a|_1^+, V_a|_2^+, V_a|_3^+ ...\}$ is strictly decreasing with $V_a|_k^+ \to 0$ as $k \to \infty$.

Thus, the closed-loop hybrid system is locally asymptotically stable if the PD gains are chosen such that $\mathbf{A}$ is Hurwitz and that the continuous-phase convergence rate is sufficiently fast such that Eq. (35) holds for any $\mathbf{x}|_0^+ \in B_{d_2}(\mathbf{0})$.

6.5 Proof of Corollary 16

PROOF. By the definition of V_a in Eq. (24), $V_a(\mathbf{x}, y_{st} - y_{std}) := V(\mathbf{x}) + \sigma(y_{st} - y_{std})^2$, where σ is positive and $V(\mathbf{x})$ and $(y_{st} - y_{std})^2$ are all bounded and nonnegative. From the proof of Theorem 14, the Lyapunov function $V_a \to 0$ as $t \to \infty$. Thus, $(y_{st} - y_{std})^2 \to 0$ as $t \to \infty$; that is, $y_{st} \to y_{std}$ as $t \to \infty$.

6.6 Proof of Corollary 18

PROOF. When the closed-loop system in Eq. (10) is asymptotically stable, the state $\mathbf{x}$ reaches zero at the steady state. From Eq. (29) in the proof of Theorem 14, the fictitious state satisfies $\|\tilde{\mathbf{x}}(\tau_k; T_{k-1}^+, \mathbf{x}|_{k-1}^+)\| \leq \sqrt{\frac{c_2}{c_1}} e^{-\frac{c_3}{2c_2}(\tau_k - T_{k-1})} \|\mathbf{x}|_{k-1}^+\| \to 0$ as $k \to \infty$. Accordingly, by Eq. (21), we have $|T_k - \tau_k| \leq L_{T_x} \|\tilde{\mathbf{x}}(\tau_k; T_{k-1}^+, \mathbf{x}|_{k-1}^+)\| \to 0$ as $k \to \infty$; that is, $T_k \to \tau_k$ as $k \to \infty$.

7 Simulations and Experiments

This section presents the simulation and experimental validation results on a ROBOTIS OP3 bipedal robot (Fig. 2).

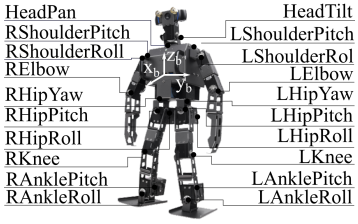

Fig. 2. An illustration of the 20 joints of a ROBOTIS OP3 robot. Its height is 500 mm. The weight is 3.5 kg. The motor stall torque is 4.1 Nm.

7.1 Trajectory Generation

This subsection explains the motion planning method utilized to generate the desired trajectories that the OP3 robot should reliably track in simulations and experiments.

The OP3 robot has 20 joint motors and 20 joints (8 upper-body joints and 12 leg joints), and thus can be fully actuated during a continuous phase. With full actuation, the robot's 12 leg joints can be directly commanded to track 12 desired trajectories, which are: 1) the desired global-position trajectories x_d and y_d and 2) the desired function $\boldsymbol{\phi}_d$.

Here, $\boldsymbol{\phi}_d$ is chosen as the desired trajectories for the following 10 control variables $\boldsymbol{\phi}_c$:

a) The pelvis height (z_b).
b) The pelvis roll, pitch, and yaw angles (ϕ_b, θ_b, ψ_b),
c) The swing-foot roll, pitch, and yaw angles (ϕ_{sw}, θ_{sw}, ψ_{sw}).

In this study, the task of motion planning reduces to the generation of the desired lateral base position y_d and the desired function $\boldsymbol{\phi}_d$, because it is assumed that the center line of the desired global path on the walking surface Γ_d is the X_w-axis and that the desired position trajectory long the path $x_d(t)$ has been provided by a high-level path planner.

Without loss of generality, the desired lateral base position y_d is chosen as the following simple sinusoidal function to represent the oscillatory global motion about the center line Γ_d during 3-D walking: $y_d(\bar{x}_b) := \alpha_1 sin(\alpha_2 \bar{x}_b + \alpha_3)$, where $\boldsymbol{\alpha} := \begin{bmatrix} \alpha_1 & \alpha_2 & \alpha_3 \end{bmatrix}^T \in \mathbb{R}^3$ is an unknown vector to be optimized.

The desired function $\boldsymbol{\phi}_d(\theta)$ is chosen as Bézier curves [36]: $\boldsymbol{\phi}_d(\theta) := \sum_{k=0}^{M} \mathbf{a}_k \frac{M!}{k!(M-k)!} s(\theta)^k (1-s(\theta))^{M-k}$, where $M \in \mathbb{N}^+$ is the order of the Bézier curves, $s(\theta) := \frac{\theta-\theta^+}{\theta^- - \theta^+}$, $\mathbf{a}_k \in \mathbb{R}^{n-2}$ is the unknown vector to be optimized, and θ^+ and θ^- are the planned values of θ at the beginning and the end of a step, respectively.

Optimization techniques are utilized to generate the desired lateral base position y_d and the desired function $\boldsymbol{\phi}_d$ with $\boldsymbol{\alpha}$ and $\mathbf{a}_k$ as optimization variables and with the following constraints enforced:

(C1) Assumptions 4-6 and the proposed conditions required to construct impact invariance construction (i.e., conditions (B1)-(B3)).
(C2) Feasibility constraints such as joint-position limits, joint-torque limits, and ground-contact constraints.

As the focus of this study is on controller design, this list of constraints is not intended to be exhaustive. MATLAB command *fmincon* is used to solve the optimization problem.

In all simulations and experiments, the same desired trajectories y_d and $\boldsymbol{\phi}_d$ are used, which corresponds to a walking pattern as illustrated in Fig. 3. The center line Γ_d of the desired path is the X_w-axis of the world reference frame. Two sets of the desired position trajectory $x_d(t)$ are considered, one with a constant velocity and the other with a time-varying velocity:

a) $x_d(t) = 4.4t - 3$ cm.
b) $x_d(t) = 3.1t - 1.5 + 1.5\sin(0.3t) - \sin(0.8t)$ cm.

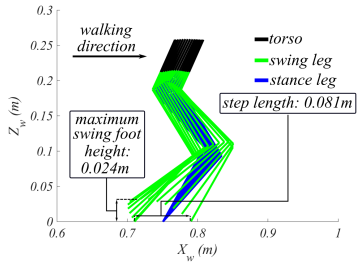

Fig. 3. An illustration of the desired walking pattern of the leg joints in the sagittal plane.

7.2 MATLAB Simulations

To validate the theoretical controller design, MATLAB is utilized to implement the control law based on a full-order dynamic model of the OP3 robot. The control gains are set as $\mathbf{K}_P = 225 \cdot \mathbf{I}_{20\times 20}$ and $\mathbf{K}_D = 30 \cdot \mathbf{I}_{20\times 20}$, which guarantee the matrix $\mathbf{A}$ is Hurwitz.

MATLAB simulation results are shown in Figs. 4-6. Figure 4 shows the capability of the proposed control law in accurately realizing the virtual constraints.

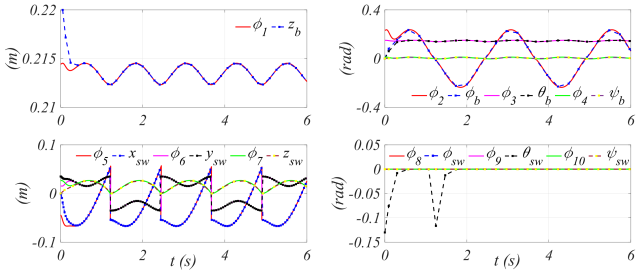

Fig. 4. Asymptotic walking pattern tracking in MATLAB simulation. The functions ϕ_i ($i \in \{1,2,...10\}$) are the elements of the desired function $\boldsymbol{\phi}_d$.

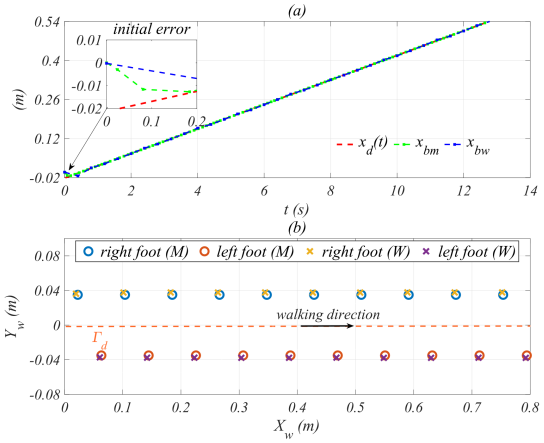

Fig. 5. Global-position tracking results in MATLAB and Webots simulations with $x_d(t) = 0.044t - 0.03$ m.

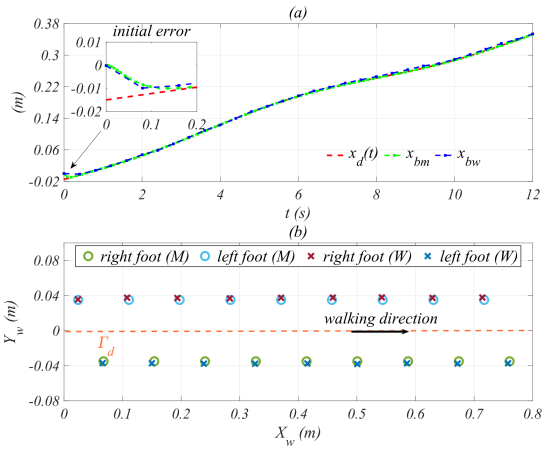

Fig. 6. Global-position tracking results in MATLAB and Webots simulations with $x_d(t) = 0.031t - 0.015 + 0.015\sin(0.3t) - 0.01\sin(0.8t)$ m.

The global-position tracking results are displayed in Figs. 5 and 6, which demonstrate that the proposed control law can drive the robot to asymptotically converge to the desired position trajectory x_d while moving along the center line Γ_d. Figures 5 (a) and 6 (a) show the position tracking results of x_d. x_{bm} is the actual global-position trajectory along Γ_d, which asymptotically converges to $x_d(t)$ in both plots. Figures 5 (b) and 6 (b) show the global-path tracking results. *left foot (M)* and *right foot (M)* are the actual stance-foot positions, which indicate asymptotic tracking of the center line Γ_d of the desired path.

7.3 Webots Simulations

To implement the proposed controller on a physical OP3 robot, the ROS package (*op3_manager*) developed by OP3's manufacturer was used in the experiments. One controller implementation limitation of OP3 is that it does not allow users to access the output torques of joint motors when the ROS package is used for controller implementation. Instead, users can only send desired joint-position trajectories to individual joints and specify the PD gains of OP3's default joint controllers. This hardware limitation is common for today's bipedal humanoid robots [1]. As the proposed control law in Eq. (8) is a torque command, this hardware limitation prevents direct implementation of the proposed control law on OP3. Thus, a controller implementation procedure is introduced to adapt the proposed control law for its implementation on the robot.

To gain preliminary insights into the effectiveness of the proposed controller implementation procedure, a Webots simulator is used to simulate a 3-D realistic robot model that closely emulates OP3's graphical, physical, and dynamical properties including its limited actuator accessibility.

Since OP3's default joint controllers only allow users to send desired joint-position trajectories to individual joints, the proposed controller implementation procedure includes: a) to generate the desired position trajectory for individual joints $\mathbf{q}_d(t)$ and b) to send the desired trajectory to the default position controllers of the corresponding joints. The overall steps of this procedure are summarized as follows:

Step 1: At the time step t, the nominal phase variable is computed as $\theta_d := x_d(t) - x_{st}$.
Step 2: The desired joint position $\mathbf{q}_d(t)$ is computed by solving inverse kinematics.
Step 3: $\mathbf{q}_d$(t) is fed into the joint controllers, which emulate the default joint controllers of a physical OP3 robot.

A flow chart of the procedue is shown in Fig. 7.

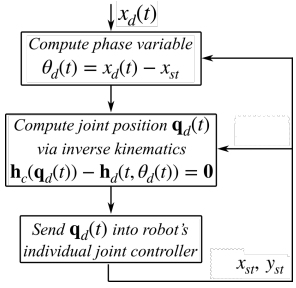

Fig. 7. A flow chart of the proposed controller implementation.

This controller implementation procedure guarantees that the desired joint trajectory $\mathbf{q}_d(t)$ preserves the feasibility and desired features of the original desired trajectories as specified in (C1)-(C3). Thus, by reliably tracking $\mathbf{q}_d(t)$ using the default joint controllers, the robot can reliably track the original desired trajectories.

Webots simulation results of the adapted controller are shown in Figs. 5 and 6. x_{bw} is the actual global-position trajectory along Γ_d obtained in Webots simulations, and *left foot (W)* and *right foot (W)* are the actual stance-foot positions in Webots simulations. For the convenience of comparison, the Webots results are displayed together with the MATLAB results.

Due to the discrepancies in the implemented controllers and robot models, Webots simulations show a nonzero steady-state tracking error instead of asymptotic tracking as demonstrated in MATLAB simulation results. However, the bounded, relatively small tracking error obtained in Webots simulations indicates the effectiveness of the proposed controller implementation procedure in guaranteeing reliable trajectory tracking in the presence of robot hardware limitations and modeling errors.

7.4 Experiments

This subsection presents the experimental validation of the proposed control approach on a physical OP3 robot. The controller implementation procedure validated through Webots simulations is utilized to guide the experiments.

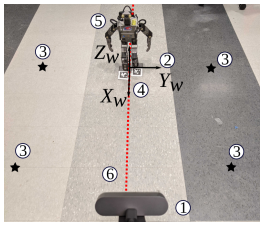

Fig. 8. Experimental set-up for assessing the performance of the proposed global-position tracking control approach on a bipedal humanoid robot. ①: a Logitech 4K PRO WEBCAM. ②: the reference points for perspective transformation. ③: an OP3 robot. ④: AprilTag attached on OP3's feet, which is used to help determine the robot's global position. ⑤: the world reference frame $\Sigma_{X_wY_wZ_w}$. ⑥: the center line Γ_d of the desired global path.

The experimental set-up is shown in Fig. 8. With this set-up, the robot's joint angles can be directly measured by joint encoders, and its global position and orientation can be determined by: a) using the 4K PRO WEBCAM and AprilTag to obtain the stance-foot position and orientation in the world reference frame and b) using the obtained stance-foot position and orientation to solve for the robot's global position and orientation via forward kinematics.

Figure 9 shows the robot's gait obtained in Webots simulations and experiments. The similarity indicates the validity of using Webots simulations to provide preliminary insights into experiments. Videos of the experiments can be accessed at https://youtu.be/VJbLMkOG_xo.

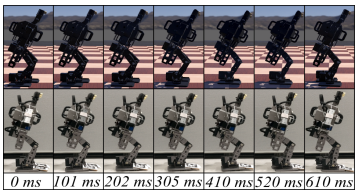

Fig. 9. Gait comparison between the experiment and Webots simulation.

Experiment results of OP3 walking on a concrete floor is shown in Fig. 10. The initial tracking error of x_d is 3 cm, which is approximately $1/3$ of a nominal step length. Due to common uncertainties during real-world robot operations, such as hardware limitations, modeling errors, and floor surface imperfections, achieving a zero steady-state tracking error may not be feasible. Thanks to the inherent robustness of feedback control, the proposed control approach can still achieve a bounded steady-state tracking error, although uncertainties are not explicitly addressed in the proposed theoretical controller design. As illustrated in Fig. 10 (a), the robot's actual global position x_{wGPT} converges to a relatively small neighborhood about the desired global-position trajectory x_d within 3 seconds. Also, despite an initial path tracking error of 5 cm, the robot remains close to the center line Γ_d of the desired global path, as indicated by the footstep trajectories (*left foot (wGPT)* and *right foot (wGPT)*) in Fig. 10 (b).

To test the limit of the inherent robustness of the proposed control approach, experiments of OP3 walking on a relatively slippery tile floor were conducted. The tracking result is shown in Fig. 11. As the surface of the tile floor was relatively more slippery than the concrete floor, the robot's stance foot slipped more frequently on the tile floor, causing a stronger violation of the modeling assumption. Thus, the steady-state tracking errors obtained from tile-floor walking were relatively larger than concrete-floor walking, as shown in Figs. 10 and 11.

Comparative experimental results of previous orbitally stabilizing controllers for 3-D fully actuated walking [1] are also displayed in Figs. 10 and 11. The figures show that the previous controller can achieve accurate *global-velocity* tracking; that is, the derivative of the robot's actual global position x_{wGPT} is close to the desired velocity. However, as indicated by the relatively large deviation of the footstep trajectories (*left foot (w/oGPT)* and *right foot (w/oGPT)*) from Γ_d, accurate global-position tracking was not guaranteed.

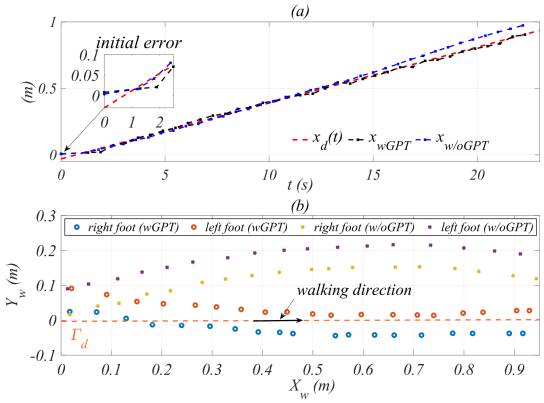

Fig. 10. Experimental results of global-position tracking on a flat concrete floor with $x_d(t) = 0.044t - 0.03$ m.

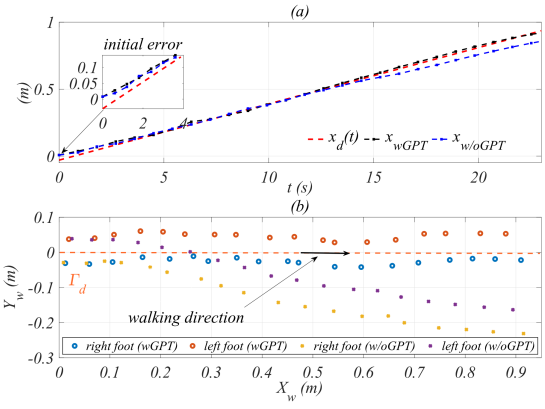

Fig. 11. Experimental results of global-position tracking on a flat tile floor with $x_d(t) = 0.044t - 0.03$ m.

8 Discussions

This section discusses our future work on extending the proposed controller design for enabling global-position tracking

over complex terrains as well as for improving robustness against uncertainties.

To realize bipedal walking on a 3-D terrain, the proposed control approach will be integrated with online motion planning in our future work. Enabling online planning of complex motions, such as bipedal walking on a 3-D terrain, is difficult mainly due to the high computational burden of planning and the limited computing capabilities of a robot. The burden could be caused by the equality constraint that a planner enforces to satisfy the proposed impact invariance construction. To alleviate the burden, the equality constraint can be relaxed to be an inequality constraint for allowing bounded violation of impact invariance. The control objective will accordingly be updated as achieving a bounded steady-state tracking error instead of asymptotic tracking. The proposed stability analysis will then be extended to derive sufficient conditions that a control law should satisfy in order to guarantee the given steady-state tracking error bound.

Due to uncertainties such as modeling errors and terrain irregularities, achieving asymptotic tracking may not be realistic during real-world robot operations. If the uncertainties are relatively small, then a bounded final tracking error can be reached by the proposed control approach, as demonstrated by the experiment results. However, if the uncertainties are relatively large, then the proposed control approach may not be able to guarantee a reliable tracking performance because uncertainties are not explicitly addressed in the current design. One potential approach to explicitly addressing uncertainties is to integrate the proposed control approach with adaptive and robust control so as to allow online model estimation as well as better disturbance rejection. For example, a control Lyapunov function could be incorporated into the proposed multiple Lyapunov function analysis to synthesize adaptive robust control laws for realizing accurate global-position tracking under uncertainties.

9 Conclusions

This paper has introduced a control approach that explicitly addresses the hybrid robot dynamics for achieving asymptotic global-position tracking during fully actuated 3-D bipedal walking on flat surfaces. With the output function designed as the tracking error of the desired global-position trajectory and virtual constraints, a continuous input-output linearizing control law was synthesized to asymptotically drive the output function to zero during continuous phases. The construction of conditional impact invariance was introduced for informing the design of virtual constraints such that the robot's desired motions defined by the virtual constraints as well as the desired global-position trajectory respect the discrete landing impact dynamics. Sufficient conditions were derived through Lyapunov analysis under which the proposed continuous control law provably guarantees the asymptotic tracking performance of the hybrid closed-loop system. Simulation and experimental results demonstrated the effectiveness of the proposed control approach in realizing asymptotic global-position tracking during 3-D walking.

References

[1] A. D. Ames, E. A. Cousineau, and M. J. Powell. Dynamically stable bipedal robotic walking with nao via human-inspired hybrid zero dynamics. In *Proc. ACM Int. Conf. Hybrid Syst.: Comput. Control*, pages 135–144, 2012.

[2] D. D Bainov and P. S. Simeonov. *Impulsive differential equations: Periodic solutions and applications*, volume 66. CRC Press, 1993.

[3] J. J. B. Biemond, N. van de Wouw, W. Heemels, and H. Nijmeijer. Tracking control for hybrid systems with state-triggered jumps. *IEEE Trans. Autom. Control*, 58(4):876–890, 2012.

[4] M. S. Branicky. Multiple Lyapunov functions and other analysis tools for switched and hybrid syst. *IEEE Trans. Autom. Control*, 43(4):475–482, 1998.

[5] A. Costalunga and L. Consolini. Synthesis of virtual holonomic constraints for obtaining stable constraint dynamics. *Automatica*, 93:262–273, 2018.

[6] X. Da and J. Grizzle. Combining trajectory optimization, supervised machine learning, and model structure for mitigating the curse of dimensionality in the control of bipedal robots. *Int. J. Robot. Res.*, 38(9):1063–1097, 2019.

[7] X. Da, O. Harib, R. Hartley, B. Griffin, and J. W. Grizzle. From 2D design of underactuated bipedal gaits to 3D implementation: Walking with speed tracking. *IEEE Access*, 4:3469–3478, 2016.

[8] F. Forni, A. R. Teel, and L. Zaccarian. Follow the bouncing ball: Global results on tracking and state estimation with impacts. *IEEE Trans. Autom. Control*, 58(6):1470–1485, 2013.

[9] Y. Gao and Y. Gu. Global-position tracking control of a fully actuated NAO bipedal walking robot. In *Proc. Amer. Control Conf.*, pages 4596–4601, 2019.

[10] C. Golliday and H. Hemami. An approach to analyzing biped locomotion dynamics and designing robot locomotion controls. *IEEE Trans. Autom. Control*, 22(6):963–972, 1977.

[11] A. Goswami, B. Espiau, and A. Keramane. Limit cycles in a passive compass gait biped and passivity-mimicking control laws. *Auto. Robot.*, 4(3):273–286, 1997.

[12] B. Griffin and J. Grizzle. Nonholonomic virtual constraints and gait optimization for robust walking control. *Int. J. Robot. Res.*, 36(8):895–922, 2017.

[13] J. Grizzle, G. Abba, and P. Plestan. Asymptotically stable walking for biped robots: Analysis via systems with impulse effects. *IEEE Trans. Autom. Control*, 46(1):51–64, 2001.

[14] J. W. Grizzle, C. Chevallereau, R. W. Sinnet, and A. D. Ames. Models, feedback control, and open problems of 3D bipedal robotic walking. *Autom.*, 50(8):1955–1988, 2014.

[15] Y. Gu, B. Yao, and C. S. G Lee. Bipedal gait recharacterization and walking encoding generalization for stable dynamic walking. In *Proc. IEEE Int. Conf. Robot. Automat.*, pages 1788–1793, 2016.

[16] Y. Gu, B. Yao, and C. S. G Lee. Exponential stabilization of fully actuated planar bipedal robotic walking with global position tracking capabilities. *J. Dyn. Syst. Meas. Control*, 140(5):051008, 2018.

[17] Y. Gu, B. Yao, and C. S. G. Lee. Straight-line contouring control of fully actuated 3-D bipedal robotic walking. In *Proc. Amer. Control Conf.*, pages 2108–2113, 2018.

[18] K. A. Hamed and A. D. Ames. Nonholonomic hybrid zero dynamics for the stabilization of periodic orbits: Application to underactuated robotic walking. *IEEE Trans. Control Syst. Tech.*, 2019.

[19] K. A. Hamed and J. W. Grizzle. Event-based stabilization of periodic orbits for underactuated 3-D bipedal robots with left-right symmetry. *IEEE Trans. Robot.*, 30(2):365–381, 2014.

[20] Y. Hürmüzlü and G. D. Moskowitz. The role of impact in the stability of bipedal locomotion. *Dyn. Stability Syst.*, 1(3):217–234, 1986.

[21] S. Kajita, F. Kanehiro, K. Kaneko, K. Fujiwara, K. Harada, K. Yokoi, and H. Hirukawa. Biped walking pattern generation by using preview control of Zero-Moment Point. In *Proc. IEEE Int. Conf. Robot. Automat.*, pages 1620–1626, 2003.

[22] H. K. Khalil. *Nonlinear control*. Prentice Hall, 1996.

[23] J.-Y. Kim, I.-W. Park, and J.-H. Oh. Experimental realization of dynamic walking of the biped humanoid robot KHR-2 using zero moment point feedback and inertial measurement. *Advanced Robot.*, 20(6):707–736, 2006.

[24] S. Kolathaya. Local stability of PD controlled bipedal walking robots. *Automatica*, 114:108841, 2020.

[25] L. Menini and A. Tornambè. Asymptotic tracking of periodic trajectories for a simple mechanical system subject to nonsmooth impacts. *IEEE Trans. Autom. Control*, 46(7):1122–1126, 2001.

[26] A. Mohammadi, M. Maggiore, and L. Consolini. Dynamic virtual holonomic constraints for stabilization of closed orbits in underactuated mechanical systems. *Automatica*, 94:112–124, 2018.

[27] B. Morris and J. W. Grizzle. Hybrid invariant manifolds in systems with impulse effects with application to periodic locomotion in bipedal robots. *IEEE Trans. Autom. Control*, 54(8):1751–1764, 2009.

[28] R. Naldi and R. G. Sanfelice. Passivity-based control for hybrid systems with applications to mechanical systems exhibiting impacts. *Automatica*, 49(5):1104–1116, 2013.

[29] Q. Nguyen, A. Hereid, J. W. Grizzle, A. D. Ames, and K. Sreenath. 3D dynamic walking on stepping stones with control barrier functions. In *Proc. IEEE Conf. Decis. Control*, pages 827–834, 2016.

[30] N. A. Radford, P. Strawser, K. Hambuchen, J. S. Mehling, W. K. Verdeyen, A. S. Donnan, J. Holley, J. Sanchez, V. Nguyen, L. Bridgwater, et al. Valkyrie: NASA's first bipedal humanoid robot. *J. Field Robot.*, 32(3):397–419, 2015.

[31] A. Ramezani, J. W. Hurst, K. A. Hamed, and J. W. Grizzle. Performance analysis and feedback control of ATRIAS, a three-dimensional bipedal robot. *J. Dyn. Syst., Meas., Control*, 136(2):021012, 2014.

[32] M. Rijnen, E. de Mooij, S. Traversaro, F. Nori, N. van de Wouw, A. Saccon, and H. Nijmeijer. Control of humanoid robot motions with impacts: Numerical experiments with reference spreading control. In *Proc. IEEE Int. Conf. Robot. Automat.*, pages 4102–4107, 2017.

[33] M. Rijnen, A. T. van Rijn, H. Dallali, A. Saccon, and H. Nijmeijer. Hybrid trajectory tracking for a hopping robotic leg. *IFAC-PapersOnLine*, 49(14):107–112, 2016.

[34] M. Vukobratović, B. Borovac, and D. Šurdilović. Zero moment point-proper interpretation and new applications. In *Proc. IEEE Int. Conf. Human. Robot.*, pages 237–244, 2001.

[35] E. R. Westervelt, J. W. Grizzle, C. Chevallereau, J. H. Choi, and B. Morris. *Feedback control of dynamic bipedal robot locomotion*, volume 28. CRC press, 2007.

[36] E. R. Westervelt, J. W. Grizzle, and D. E. Koditschek. Hybrid zero dynamics of planar biped walkers. *IEEE Trans. Autom. Control*, 48(1):42–56, 2003.